Thermocurrents and their role in high Q cavity performance

R. Eichhorn,* C. Daly, F. Furuta, A. Ganshyn, M. Ge, D. Gonnella, D. Hall, V. Ho, G. H. Hoffstaetter, M. Liepe, J. May-Mann, T. O'Connell, S. Posen, P. Quigley, J. Sears, and V. Veshcherevich

CLASSE, Cornell University, Ithaca, New York 14853, USA

(Received 12 January 2015; published 19 January 2016)

Over the past years it became evident that the quality factor of a superconducting cavity is not only determined by its surface preparation procedure, but is also influenced by the way the cavity is cooled down. Moreover, different data sets exist, some of which indicate that a slow cooldown through the critical temperature is favorable while other data states the exact opposite. Even though there were speculations and some models about the role of thermocurrents and flux-pinning, the difference in behavior remained a mystery. In this paper we will present a consistent theoretical model which we confirmed by data that describes the role of thermocurrents, driven by temperature gradients and material transitions. We will clearly show how they impact the quality factor of a cavity, discuss our findings, relate it to findings at other labs and develop mitigation strategies which especially address the issue of achieving high quality factors of so-called nitrogen doped cavities in horizontal tests.

DOI: 10.1103/PhysRevAccelBeams.19.012001

I. INTRODUCTION

Continuous wave mode operation of future accelerators like ERLs or the LCLS-II [1] have driven the research on achieving high quality factor superconducting radio frequency (SRF) cavities to keep operation cost low. As the surface resistance of superconducting cavities approaches the theoretical limits parasitic effects limiting the performance came into focus of research. One interesting finding was that the quality factor of a cavity is impacted by the cooldown rate.

This effect was first reported in 2011 by HZB [2,3] and later refined in [4]: The papers state that an increase in surface resistance proportional to the temperature difference during cool-down is observed and it was postulated that trapped flux generated by thermocurrents was responsible for the effect. Conversely, an even cool-down without thermogradients prevented the generation of additional trapped flux due to the thermoelectric effect and hence preserved the high-Q state. They also observed with samples that a slow cooldown can enable better external flux expulsion. The paper discussed the latter findings, but judged the latter to be not the main effect responsible for the cavity-test observations.

Similar results were gained at Cornell, seeing that an initial cooldown to 4 K, followed by a thermocycle warming to 20 K and a slow recool through the critical temperature increased the quality factor significantly [5]. In contrast to this, FNAL [6] saw an increase of the quality factor of nitrogen doped cavities after a fast cooldown. These contradictory findings have been reproduced and confirmed by others so there is no doubt about the validity of the data.

Thermocurrents have been a candidate to explain these findings for several years. Even though their existence was not in question, their impact on the cavity performance was never clearly understood. Recent experiments at Cornell and other labs performed in vertical and horizontal tests have now revealed a breaking in symmetry, allowing a consistent explanation of the data, including the deterioration of the quality factor. The focus of this paper will be the role of thermocurrents and the introduction of a model to describe asymmetric current distributions creating magnetic fields at the rf surface of the cavity.

II. BACKGROUND

During cavity testing inside Cornell's Horizontal Test Cryostat (HTC), performed in the framework of our ERL R&D we confirmed a very interesting effect: The quality factor Q of a superconducting cavity can be increased after the initial cooldown (which was done with a rate of $\sim$3 K/h around the critical temperature) by going through a second cooldown cycle which warms up the cavity to 15–20 K and then slowly cools it back to 2 K again, transiting the critical temperature with a change rate as low as 0.5 K/h.

By this cycle, we were able to increase the Q at 1.8 K from 3.5×10^{10} to 6×10^{10}. This has already been reported in [7]. In the absence of having a good understanding of these findings, several possible explanations were investigated. To check if the shielding efficiency of the magnetic shielding enclosing the cavity (and ensuring an appropriate damping of the earth magnetic field in the vicinity of the

r.eichhorn@cornell.edu

cavity) is deteriorated during the cooldown, we started to equip our test setup with a cryogenic flux gate magnetometer that measured the magnetic field close to the cavity inside the inner magnetic shielding [8]. Interestingly enough, we found that the magnetic field changes drastically during cooldown: it started from an ambient value of 0.15 μT rising to 0.45 μT, then going down and reversing its direction (which needed a manual adjustment, resulting in some missing data, see Fig. 1 at 19:00 h) to -0.25 μT to become -0.11 μT as the cavity transits through the critical temperature T_c becoming superconducting. This behavior, depicted in Fig. 1, is clearly not compatible with a temperature dependent efficiency of the magnetic shielding.

One potential explanation of this finding is magnetic fields, induced by thermocurrents. Today's SRF cavities are made from niobium which becomes superconducting at 9.2 K. Cooled by liquid helium, these cavities are usually enclosed by a vessel made from titanium, welded to the cavity at the cutoff tubes. With both material transitions held at different temperatures, there is the potential to drive a persistent thermo-current.

However, arguments were made that thermocurrents should not lead to any magnetic field outside the helium vessel (where the magnetometer in our setup was located) nor inside the cavity (where it could affect the quality factor by means of flux trapping) [9]. The arguments were based on symmetry, solving Maxwell's equations analytically and potential asymmetries were only rated a minor effect. Similar arguments were used in [4] even though their analysis relies on magnetic fields at the rf surface to explain the observed changes in Q but leaving the reasons for these fields as on open question.

We recently found conditions, under which this symmetry is strongly broken, that completely change the perspective under which thermocurrents have to be seen.

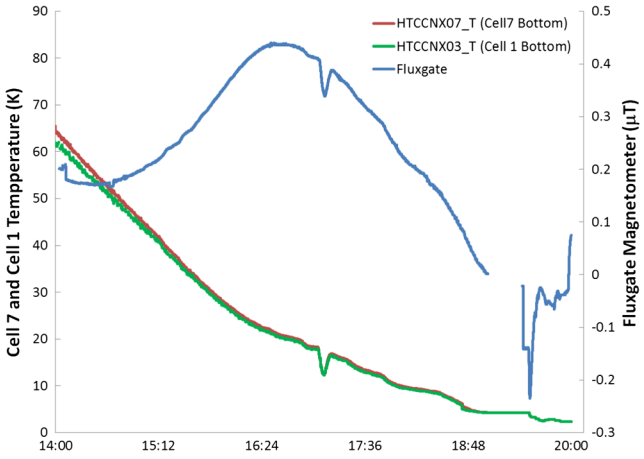

FIG. 1. Magnetic field measurement during initial cooldown of a cavity in a horizontal test (at 3.2 K/h around T_c). The flux gate magnetometer was mounted outside the helium tank but inside the second layer of magnetic shielding, measuring only one (arbitrary) component of the magnetic field.

When analyzing data from different sources one should be aware that cavity testing can also be conducted in a bath cryostat where the cavity is not necessarily enclosed by a Ti-vessel. Even though vertical tests are usually conducted with bare cavities while horizontal test require cavities with Ti-vessel, the effect from horizontal or vertical cooling has to be clearly distinguished, as we describe below.

III. SEEBECK EFFECT

Thermocurrents are the result of the Seebeck effect, which is well known in physics for more than a century: Discovered in 1826, Seebeck found that a current will flow in a closed circuit made of two dissimilar metals when the two junctions are maintained at different temperatures. However, the effect also exists within a single, uniform metal, where a voltage potential builds up between the warmer and the colder end of the material.

The polarity and the value of that emf voltage is dependent on the material, leading to the definition of the Seebeck coefficient S:

$$\Delta U = S \cdot \Delta T. \tag{1}$$

Seebeck coefficients of metals can have either sign as they are defined relative to platinum. In a single metal arrangement, depicted by Fig. 2 (left), this voltage exists across the metal but does not result in a current flowing other than simply building up the charges, initially. If there is a material transition, where two different metals are joined, not only does a potential difference exist, but it might also drive a persistent current (driven by the temperature difference) if the loop is closed (see Fig. 2, right diagram).

As superconducting cavities are made out of niobium while the helium vessel enclosing them is typically titanium this effect is relevant for accelerator physics: During the cooldown of a dressed cavity (a cavity welded into its helium vessel) it is easy to imagine that both ends of the

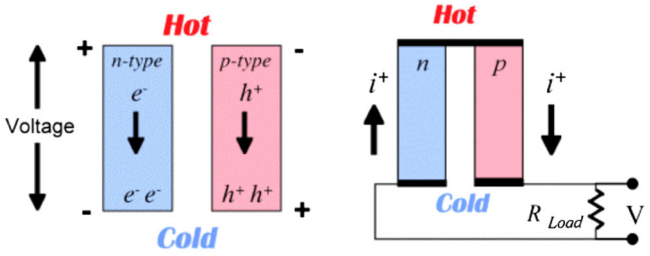

FIG. 2. Visualization of the Seebeck voltage of different metals (taken from [10]), not connected (left) and connected on one side (right). In the nonconnected case a static voltage builds up resulting in a vanishing current in the equilibrium. If a loop exist (connected scenario), a persistent current is excited even in the equilibrium state, driven by the temperature difference between both material transitions.

TABLE 1. Thermoelectric power (Seebeck coefficient) for niobium and titanium, taken from [11]. Values are given in μV/K.

	10 K	20 K	50 K	80 K	100 K
Nb	0.31	0.98	2.73	3.09	3.13
Ti	N/D	N/D	−3.00	−3.00	−2.60

cavity (where the Nb-Ti transition is located) have different temperatures.

The emf voltage following the Seebeck theory is then given by

$$U_{\mathrm{th}} = (S_{\mathrm{Nb}} - S_{\mathrm{Ti}}) \cdot \Delta T. \tag{2}$$

Seebeck coefficients are usually also temperature dependent. With the more general definition of the Seebeck coefficient, the thermovoltage becomes

$$U_{\mathrm{th}} = \int_{T_1}^{T_2} [S_{\mathrm{Nb}}(T) - S_{\mathrm{Ti}}(T)] dT. \tag{3}$$

The data for niobium and titanium, taken from [11] are given in Table I. Below 50 K the thermoelectric power of titanium is unknown. As the Seebeck effect vanishes for all materials at zero temperature, one assumption would be to proclaim a linear dependency of the coefficient with temperature between 0 K and the first data point at 50 K.

During the reviewing process of this paper, new data on the thermoelectric power was published [12] which confirmed a linear behavior of the Seebeck coefficient of Titanium, but also indicated a potentially nonlinear behavior of Niobium (Fig. 9 in [12] at temperatures below 25 K, large sample data).

IV. THERMOCURRENT TEST SETUP

To investigate the Seebeck effect in detail and to confirm the thermoelectric power of titanium and niobium below 50 K, we built a window-frame setup, as shown in Fig. 3. It follows a similar setup used by HZB [3] to investigate thermocurrent generated flux trapping.

The setup simulates a cavity/vessel arrangement by having two transitions between niobium and titanium. Each transition was equipped with a cernox® thermometer. The lower end was cooled by liquid helium and the upper end was heated. The Seebeck voltage, which is expected [Eq. (3) and Table I] to be in the order of μV, drives a current, which due to the low resistance of the circuit, given by

$$R = \frac{\rho L}{A} \tag{4}$$

is potentially in the order of one Ampere. Using published data for the resistivity of niobium [13] and titanium [14] we found the resistance of our circuit to be 370 $\mu\Omega$ at 10 K.

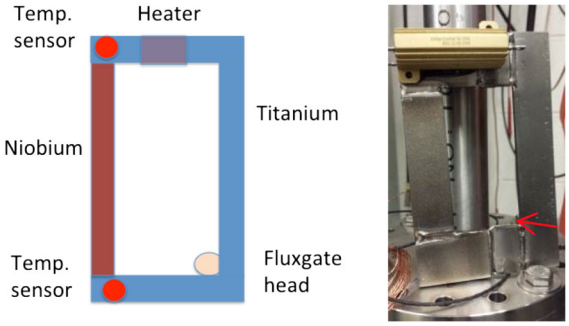

FIG. 3. Setup to measure the thermocurrents. On the left is a sketch of the arrangement with the principle components, on the right is a photograph of the setup with the arrow pointing to the location of the flux gate probe. The size of the frame was 12.5 cm by 7.75 cm on the outside and 7.5 cm by 3.75 cm inside, the thickness was 0.25 cm.

To avoid material transitions influencing the behavior of the circuit we decided to measure the current indirectly by its generated magnetic flux. A fluxgate sensor was placed in the corner of the window-frame and the analysis was guided by Biot-Savart's law

$$d\vec{B} = \frac{\mu_0}{4\pi} \frac{I d\vec{l} \times \vec{r}}{r^2}. \tag{5}$$

Simplifying the geometry to a single line of current and adding up all 4 contributions, we calculated a thermocurrent induced magnetic field at the position of the sensor (being 1.75 cm away from the geometrical center line of the window frame) of 1.03 μT for a current of 0.027 A, being expected with a temperature difference between the material transitions of 10 K.

As the heater in the setup influenced the magnetic reading due to its (small but visible) stray field we only

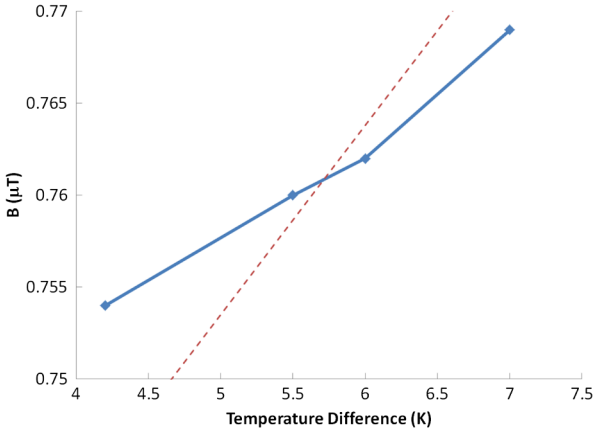

FIG. 4. Measured magnetic field as induced by the thermocurrent (solid line). The lower temperature transition was held at 9–10 K. The extrapolated field for ΔT approaching 0 K is the residual magnetic field inside the cryostat. The dashed line is the expected magnetic field using Eq. (3)–(5). For details see text.

considered data taken without current through the heater to be relevant. The result of the measurement as well as the predicted behavior is given in Fig. 4. By that, we found a very weak parabolic behavior and an almost linear dependency from the temperature difference which suggest an only weak dependency of the Seebeck coefficient from temperature. However, we measured 5 nT/K while theoretical expectations using the simplified model are 10 nT/K. More details can be found in [15]. Our results are consistent with data in [2].

V. VERTICAL CAVITY TEST DATA

In the framework of our ERL program [16] we built 6 cavities for the Main Linac Cryomodule (MLC) prototype [17]. All of them were tested vertically before the helium vessel was welded to the cavity. In order to understand the thermocurrent effect, we tested the cavity fully insulated from its support frame. A second measurement was done on two cavities after the helium vessel was welded to the cavity which then allows thermocurrents to flow.

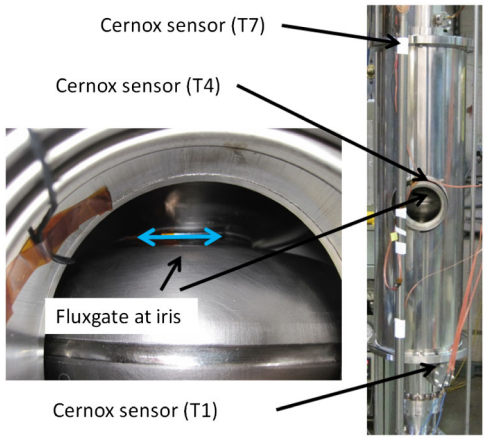

FIG. 6. Instrumentation during vertical testing of the fully dressed cavities. The fluxgate was located at the iris between cell 3 and 4, measuring the azimuthal field components. Also indicated are the positions of the thermometers.

We conducted several tests going through the critical temperature slow and fast, the results of which are shown in Fig. 5. The graph gives the magnetic field at the iris between cell 3 and 4 (which is the center of the cavity, see Fig. 6), measuring the azimuthal magnetic field, which is the expected orientation of a thermocurrent induced field. Both data sets where taken on the same dressed cavity. During the slow cooldown the temperature difference between both cavity ends was less than 0.2 K when passing T_c but as high as 30 K in the fast cooldown.

Besides the stronger fields observed on the fast cooldown there is an important difference in the data: the field remaining in the iris area was 0.1 μT for the slow cooldown

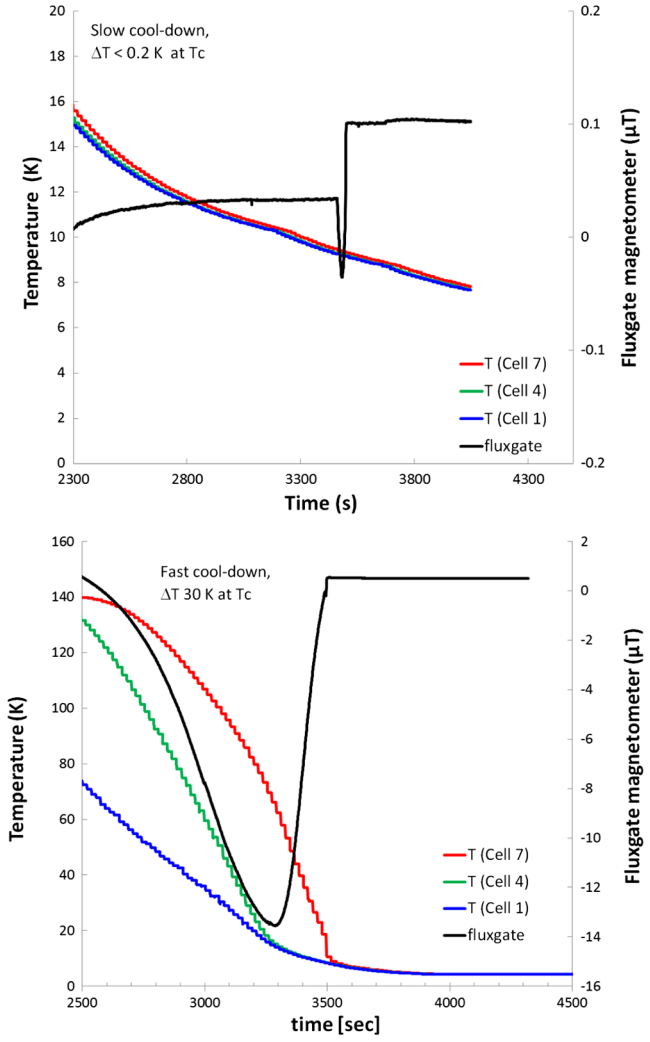

FIG. 5. Slow (upper plot) and fast (lower plot) cooldown cycle: shown are temperatures of the dressed cavity and the magnetic flux measured at the iris location. The residual azimuthal field component inside the cryostat was 0.1 μT at room temperature.

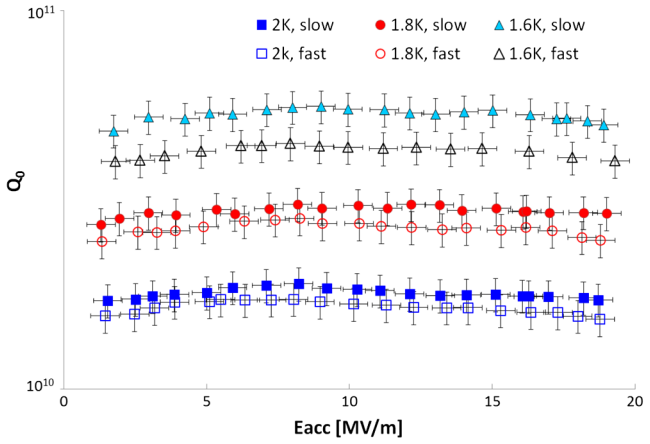

FIG. 7. Cavity Qs of the ERL7-3 cavity (dressed) for different temperatures and different cooldown cycles. The undressed cavity tested within the error bars like the dressed cavity under slow cooldown.

TABLE II. Quality factors at different temperatures measured after fast and slow cooldown on a dressed ERL cavity.

T	Q_0, fast cooldown	Q_0, slow cooldown
1.6 K	4.2×10^{10}	5.3×10^{10}
1.8 K	2.7×10^{10}	3.0×10^{10}
2.0 K	1.6×10^{10}	1.8×10^{10}

but as high as 0.53 μT after a fast cooldown. Concluding that this is the frozen flux seems to be too bold, as the kink in the data close to transition temperature reveals a rather complicated dynamics which is the subject of further investigations.

The data clearly shows higher fields are present on cooldown for a fast cycle, pointing to thermocurrents as their driver, given the fact that the temperature spread between the bottom and the top of the cavity is greater for the fast cooldown.

After each cooldown cycle, we measured the quality factor of the cavities. Figure 7 and Table II summarize the results of one of the cavities (ERL7-3). It should be noted that the cavity was not removed from the dewar between the tests. Depending on the cooldown cycle we found different Q factors with Qs higher for a slow cooldown. Using the cavity's geometric factor G of 270.7 Ω, the surface resistance has been calculated and the residual resistance has been extracted (using the method described below), leading to 4.9 nΩ for the fast cooldown and 3.7 nΩ in the case of a slow cooldown. Consistently, a reduction of 1 nΩ in the residual surface resistance has been found for a slow cooldown [18].

It should be noted that the cavities were also measured in the undressed state, fully insulated from their support frame, resulting in Qs that within the error bars agree with results on the dressed cavity after the slow cooldown.

Even though symmetry-based arguments suggest that the cavity inner surface is not affected by the magnetic field of a thermo-current [9] and thus the quality factor/residual resistance is unaffected, too, we confirmed by several measurements an increase of 1 nΩ in the residual resistance after a fast cooldown of the dressed cavity. An interpretation of that will be given below. It should be noted that these results confirm results from a conventionally treated cavity [19] and contradicts findings on nitrogen-doped cavities [6,20].

As pointed out in [9] a small deviation in the concentric alignment of the cavity/vessel assembly can lead to a symmetry breaking which is able to explain these vertical test results. However, we will show that there is a different mechanism leading to a stronger symmetry breaking which is able to also explain the bigger impact of the cooldown cycle on the residual resistance especially in horizontally oriented cavities, which we observed in later tests.

VI. HORIZONTAL TEST DATA

Cryomodule test within the LCLS-II high Q_0 program [20] allowed us to study cooldown effects on a nitrogen-doped cavity. For this test, a nitrogen-doped cavity was welded into an ILC style titanium helium vessel, and installed in the Cornell Horizontal Test Cryomodule (HTC). Magnetic field probes and temperature sensors on the cells of the cavity allowed for detailed measurements of temperature gradients and magnetic fields during cavity cooldown, including a direct measurement of the thermoelectric induced magnetic field. Figure 8 shows the location of these sensors. A heater was placed on one of the beam tubes of the cavity to generate large longitudinal gradients during cooldown, potentially resulting in a large thermovoltage, high thermocurrents and increased induced magnetic field during transition to superconductivity. The residual magnetic field during the experiment was below 0.5 μT.

A total of five fast cooldowns were completed on the cavity in the HTC. For each cooldown, Q_0 (and thus R_s) was measured versus E_{acc} at 2.0 and 1.6 K. Additionally, in the first cooldown, R_s vs T was measured between 4.2 and 1.6 K at 5 MV/m and Q_0 vs E_{acc} was measured at 1.6, 1.7, 1.8, 1.9, 2.0, and 2.1 K in 1 MV/m increments. This allowed for an extraction of BCS material properties both at low field (using R_s vs temperature data) and as a function of accelerating field. This extraction was completed by fitting to BCS theory using SRIMP [21]. Because the BCS material properties are dependent on the cavity itself and not the cooldown [22], extraction of the BCS resistance

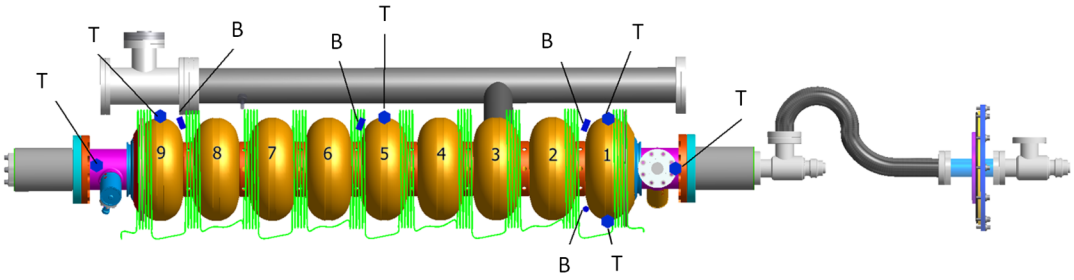

FIG. 8. Horizontal test set-up to measure a nitrogen doped cavity, indicating the location of the instrumentation (T for temperature sensors, B for fluxgate (magnetic) sensors). For determining the temperature difference along the cavity, the leftmost and rightmost sensor was used. The green contour represents a solenoid that was wound around the cavity which is of no relevance within this paper.

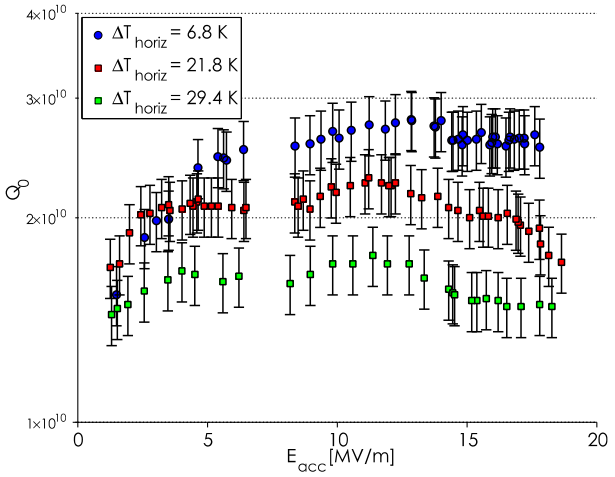

FIG. 9. Q_0 vs E_{acc} performance of an LCLS-II N-doped 9-cell cavity at 2.0 K in the Cornell Horizontal-Test Cryomodule for different temperature gradients between the cavity ends near T_c. Uncertainty on E_{acc} is 10%.

(temperature dependent resistance) for only the first cooldown is sufficient to determine residual resistance in all subsequent cooldowns.

We measured the quality factor of the cavity after each cooldown, as reported in Fig. 9, for the situation were no or a negligible thermocurrent is excited ($\Delta T = 6.8$ K) as well as for a medium and high thermal gradient situation ($\Delta T = 21.8$ K and 29.4 K). The quality factors we got were 2.7×10^{10} ($\Delta T = 6.8$ K), 2.0×10^{10} ($\Delta T = 21.8$ K) and 1.5×10^{10} ($\Delta T = 29.4$ K). Values quoted refer to 2 K and 16 MV/m and the geometry factor of this cavity is 278 Ω.

Figure 10 shows the extracted residual resistance as a function of horizontal temperature gradient. Above sufficiently large spatial temperature gradients (~10 K), one clearly sees the onset of additional residual resistance. It should be noted that each data point requires a warmup and cooldown which explains the limited data set. However, we

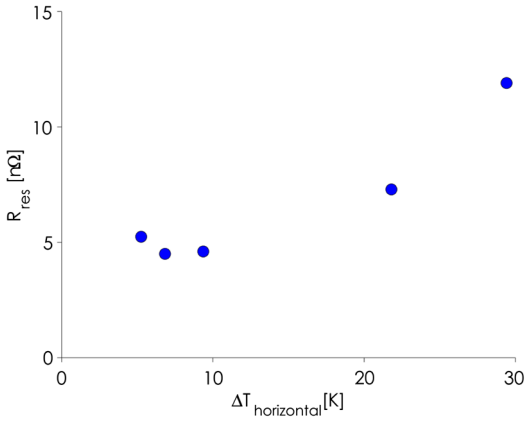

FIG. 10. Extracted residual resistance (at a field of 5 MV/m) as a function of the horizontal temperature difference, measured on a nitrogen doped cavity. Around 10 K, the effect of thermocurrents becomes noticeable.

can clearly see that at large temperature gradients, residual resistance is higher.

We have shown that the residual resistance can indeed be impacted by large horizontal temperature gradients inducing thermocurrents. So far, we still have to show why the thermocurrent induced magnetic fields that we measured between the cavity outer wall and the helium vessel impacts the rf surface of the cavity. This will be explained in the next section.

VII. THERMOCURRENT SIMULATION

Previously, analytical based arguments were made that the axial symmetry of SRF cavities leads to no (or when considering the potential asymmetry from vessel or cavity port negligible small) thermoelectric induced magnetic fields in the relevant rf penetration layer at the inner cavity surface [9]. It was concluded that therefore thermoelectric currents are not a concern for the performance of SRF cavities. However, our findings indicated early-on that thermoelectric currents may have a more severe impact on the SRF performance as so far predicted.

In order to gain a better understanding, numerical simulations with CST® EM-Studio® were undertaken. We modeled a real size cavity with a simplified helium vessel (see Figs. 11 and 12). The Seebeck voltage was applied over an artificial gap on the right side of the helium vessel, depicted by the ports visible in Figs. 13 and 14. For the simulation, realistic values for the expected thermovoltage and the resistivity of the materials were used [11,13,14] and the mesh was carefully adjusted to avoid numerical problems.

In order to understand the results, a distinction into two different cases is appropriate:

A. Azimuthally symmetric case

This scenario is depicted in Fig. 11: even though the cavity/helium-vessel may have nonuniform properties,

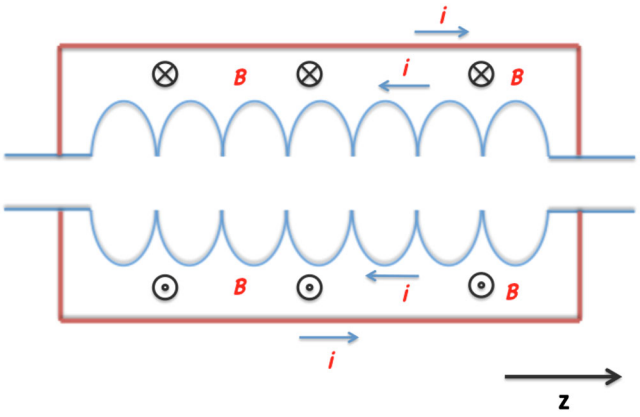

FIG. 11. Thermocurrents and associated magnetic field in the azimuthal symmetric scenario: the Seebeck induced currents i are equal, producing a symmetric magnetic field.

symmetry exists if the properties are independent of the azimuth. In this scenario, a thermocurrent is excited if a temperature gradient exists along the z-axis: The disparity of the temperatures at the material transitions results in a Seebeck voltage, driving this current.

However, due to the postulated symmetry, currents in the upper and the lower half are equal, resulting in a magnetic field that only exists between the outer cavity wall and the helium vessel. As a consequence of the vanishing magnetic field at the rf surface of the cavity, thermocurrents in this symmetric case do not result in any contribution to the flux pinning at transition.

B. Nonazimuthal symmetric case

As described, the temperature gradient along the z-axis generates the Seebeck voltage. It relates to the current over the resistivity of the circuit. If no azimuthal symmetry exists, the resistivity for example in the upper half might be higher compared to the lower half. In that case the Seebeck voltage would result in an uneven current distribution. As a result, the magnetic field distribution would also be asymmetric and magnetic fields inside the cavity will exist, as shown in Fig. 12. It is easy to imagine that during the cooldown, not only a temperature gradient between the cavity ends exists (resulting in the Seebeck voltage) but also a transversal gradient (top to bottom) which diverts the currents asymmetrically as a result of temperature dependent resistance. In the extreme case one might assume that part of the cavity is already superconducting while the remaining portion is still resistive.

C. Results

For the numerical simulation we assumed a Seebeck voltage of 150 μV, which corresponds to a temperature of 10 K on one side and 50–60 K on the other side (the calculation is based on experimental conditions as published in [20,23] and the linear extrapolation described above). We also assumed constant (which can be interpreted as a mean) resistivity for the niobium (5×10^{-10} Ωm when normal conducting) and the titanium (2.5×10^{-7} Ωm). The bellow of the titanium vessel was accounted for this simulation in terms of resistance but it was not modeled geometrically. We calculated the current in the thermo-loop to be 4.8 A and the maximum magnetic field to be 25 μT. The results for the symmetric scenario are shown in Fig. 13, where the upper plot gives the magnetic field configuration. The plots below give the magnetic field along a z-axis cut at the location of the equator (left) and the iris (right). As expected, fields are symmetric and no field inside the cavity exists.

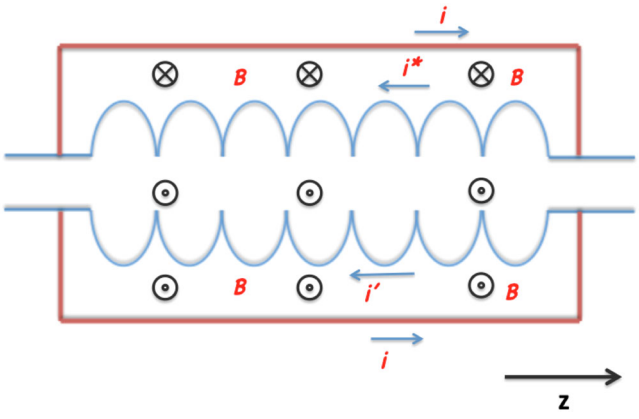

FIG. 12. Thermocurrents and associated magnetic field in the asymmetric scenario. In this case, the currents along the helium vessel are approximately equal (explained in the text) but i* and i' might not be equal, resulting in a field configuration with fields inside the cavity.

It should be noted that this plot also explains the different magnetometer readings we got related to the thermocurrents, depending on their positioning at the iris (where the field is enhanced) and the equator, where only a weaker field is measurable [15].

Simulating the asymmetric scenario we assumed conditions as above except the lower portion of the cavity now being a perfect conductor- representing its vanishing resistance in the superconducting state. The field configuration gained is given in Fig. 14 (upper plot), the lower plots are z-cuts at the iris and equator, respectively. As a result of the azimuthal asymmetry, magnetic fields are asymmetric and a reasonable large magnetic field exists inside the cavity. During transition of the upper half of the cavity through T_c, this field could potentially be trapped, causing an increase in the residual resistance and thus deterioration in the cavity Q.

Figure 14 also indicates that a measurable thermocurrent induced magnetic field is generated outside the titanium vessel. This explains our initial findings referred in Fig. 1. Given the field configuration has been simulated, this allows to probe the field at the rf surface without having to place a magnetometer inside the cavity. Assuming no other sources of thermocurrents exists, a magnetic field reading outside the helium vessel permits a direct distinction between the thermoelectric magnetic fields which do not affect performance (symmetric, no field inside the cavity nor outside the helium vessel) and the fields which impact the performance (asymmetric with field inside the cavity and outside the helium vessel).

D. Interpretation

If an azimuthal asymmetry exists, thermocurrents can generate magnetic field at the rf layer of the cavity that is subject to flux trapping. A reason for this asymmetry can be found in the cooldown, if a transversal temperature gradient in the dressed cavity exists. This is usually the case in a horizontal test, where the cavity is cooled through a stream of cold helium entering through a cooldown port at the lower portion of the helium vessel, while the exhaust is located on the top [23]. This results in a lower temperature of the lower

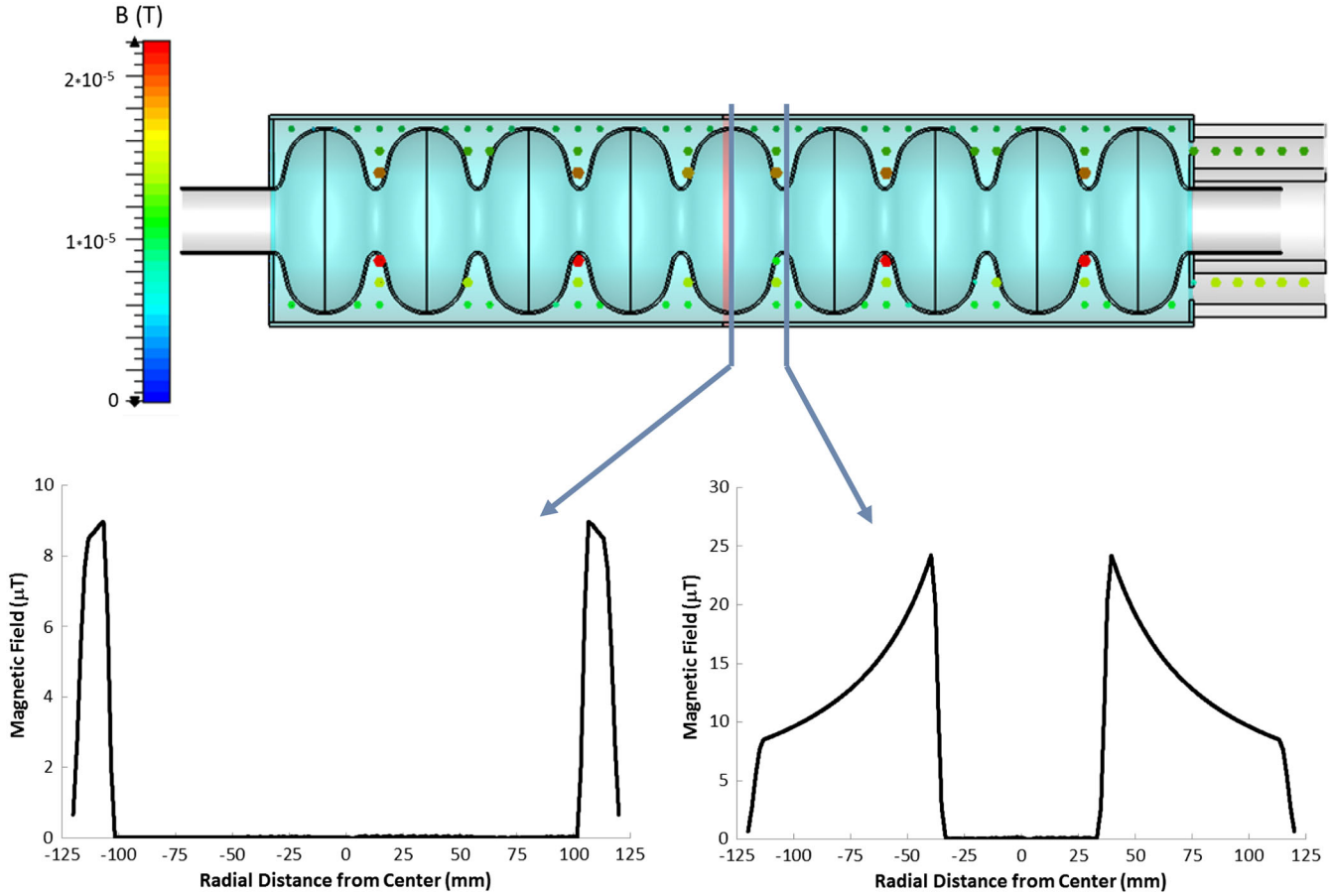

FIG. 13. Results of the numerical field simulation with the parameters given in the text, assuming azimuthal symmetry. The top graph shows the 3-D field configuration, plots below give z-axis-cuts along one equator (bottom left) and at an iris (bottom right), both locations where close to the cavity center. Positive radial distance is defined as above centerline. As expected, the magnetic field resulting from the thermocurrent fully vanish inside the cavity.

portion of the cavity with decreased resistance and increased current in that region. As the resistivity of the titanium is almost constant below 50 K [14], the change of resistance has to be caused by the niobium with the most drastic change to happen as the niobium becomes superconducting.

The thermocurrent effect has less influence in vertical tests for two reasons. First, only bare cavities are tested, but a closed current loop may exist over the cavity support frame. Longitudinal temperature gradients might be huge resulting in large thermocurrent induced magnetic fields. Second, due to the mostly preserved azimuthal symmetry as a result of the only z-dependent temperature distribution, fields are symmetric eventually generating no flux at the rf layer of the cavity.

VIII. TRANSITION DYNAMICS

The transition dynamics of a dressed cavity in a horizontal test seems to be a complicated process. As the cavity cools down, the Seebeck voltage increases due to the thermoelectric power of the two materials involved. At the same time the loop resistance decreases. Both effects lead to an increase in the current and induced magnetic field, as show in Fig. 5, lower plot, up to $t = 3300$ s (The decrease in field after $t = 3300$ s is due to the decrease in the temperature difference).

However, as the niobium becomes superconducting additional effects take place: first, the resistance of the loop will drop slightly, increasing the current. In the asymmetric scenario we calculated an increase of 5%–10%. However, the Seebeck voltage in niobium would eventually drop rapidly as a superconductor by definition does not have thermoelectric power—so the net effect might be a decrease in current and fields.

On top of that, the niobium begins to expel or pin flux. Characterized by the change in the permeability and the magnetization that goes with it, the field configuration changes. Overall, this makes it difficult to judge, which of these effects contribute to which amount to the spike, seen in Fig. 5, upper plot at $t = 3400$ s (which also exists in the lower plot at $t = 3500$ s). More detailed investigations are currently being conducted.

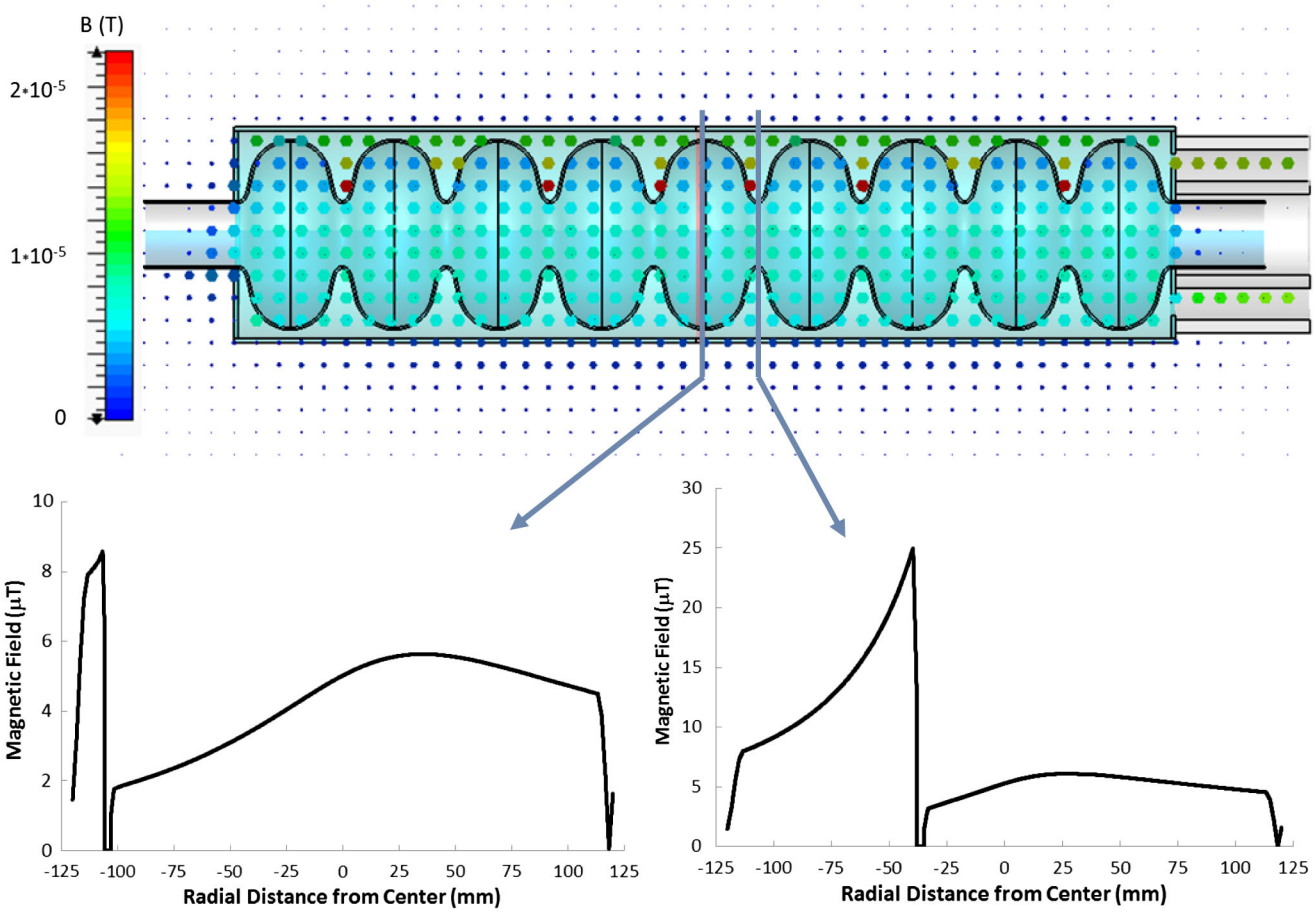

FIG. 14. Results of the asymmetric calculation, where the lower portion of the cavity is assumed to be superconducting while the upper half remains normal conducting. Again, the upper graph shows the 3-D field configuration which now is asymmetric, too. The z-axis-cuts (bottom, equator cut on the left, iris data on the right) reveal a significant amount of magnetic flux inside the cavity which at transition to superconductivity of the upper half is susceptible to pinning and as a result increasing the surface resistance.

IX. ASSYNETRIC THERMOCURRENT MITIGATION STRATEGIES

Our analysis shows that in order to minimize thermocurrents, any temperature gradients should be avoided. However, there is evidence that the cool-down has also an effect on the amount of magnetic flux trapped as the cavity becomes superconducting [24–26]. It seems, that a fast cooldown leads to less pinning at least for nitrogen doped cavities. For conventional cavities, the opposite has been stated in [2,18]. The increase of surface resistance caused by flux pining on N-doped cavities is more severe compared to conventional cavities [22]. As it stands, high cooldown rates might be required if the shielding of the cavity against residual magnetic field is insufficient. The tradeoffs between the optimum shielding, cooldown rate and ratio of symmetry have to be assessed by additional studies.

From what we know, one can state that a longitudinal temperature gradient drives the thermocurrent induced field but the transversal gradient determines how much of this flux hits the sensitive rf surface of the cavity. However, there seems to be no way to avoid a transversal gradient in a horizontal setup which means one should avoid longitudinal gradients. This is optimally achieved by having two cool-down lines feeding the both ends at the bottom of the helium vessel and a centrally located gas exhaust [27]. Both cool-down lines have to have a well-balanced helium mass flow to achieve a minimal temperature difference of the two material transitions on either end.

But there exists two more mitigation options. Our analysis showed that the resistance of the cavity slightly above T_c is $\sim$2.5 $\mu\Omega$, while the helium vessel has $\sim$30 $\mu\Omega$. Half of that resistance is coming from the bellow in the helium vessel, necessary to allow tuning of the cavity. Doubling the bellow's length would increase the resistance of the thermocurrent loop by 50% and as the Seebeck voltage is determined by the temperature difference, the resulting current and magnetic fields would decrease to 67%. Together with a well-balanced cooling scheme minimizing longitudinal gradients this might resolve the issue of trapping thermocurrent induced magnetic fields.

A rather rigorous mitigation strategy would be replacing the titanium helium vessel around the cavity by a niobium container. In lacking a material transition, thermovoltages in this arrangement would never lead to a loop current. It should be mentioned that some of the low beta cavities operated successfully (see for example [28]) have helium vessels made from reactor grade niobium with a negligible impact on overall costs.

X. CONCLUSIONS

We have investigated the effect of thermocurrents in dressed cavities and their impact on the quality factor. We demonstrate the existence of magnetic fields associated with the currents and proved their contribution to the performance, which is minor in vertical testing but can be severe in horizontal test. Our model allows an explanation of the findings which points to a longitudinal temperature difference to drive the current while the transversal gradient determines the amount of asymmetry which results in generating fields at the rf surface layer. The asymmetry can be diagnosed by a magnetometer placed outside the helium vessel assuming no additional thermocurrent loops exist. Based on this, tradeoff studies on magnetic shielding and cooldown procedures can be conducted.

ACKNOWLEDGMENTS

The authors would like to acknowledge the great boost the LCLS-II high Q R&D program gives to the field which allowed us to continue investigating the mystery of thermocurrents. Special thanks go to the Cornell cryomodule team for assembling the HTC in record time and to the cryogenics group for all their support. We also like to express our gratitude to the entire FNAL SRF group for supplying a nitrogen doped 9-cell cavity. We also would like acknowledge that during the review process of this paper the HZB group published their investigations on thermos-currents [12] coming independently to the same conclusions about the symmetry breaking process. This work has been supported by DOE Grant No. DE-ACO2-76SF00515 and NSF Grants No. PHY-1002467 and No. DMR-0807731.

[1] J. Galayda, *Proceedings of the 27th Conference on Linear Accelerator Geneva, Switzerland* (JACoW, Geneva, 2014), p. 404.

[2] J.-M. Vogt, O. Kugeler, and J. Knobloch, Impact of cooldown conditions at T_c on the superconducting rf cavity quality factor, Phys. Rev. ST Accel. Beams **16**, 102002 (2013).

[3] O. Kugeler, W. Anders, J. Knobloch, and A. Neumann, *Proceedings of SRF2011, Chicago, IL, USA* (2011), p. 724.

[4] O. Kugeler, J. Knobloch, and J. M. Vogt, *Proceedings of SRF2013, Paris, France* (2013), p. 370.

[5] N. Valles, R. Eichhorn, F. Furuta, G. M. Ge, D. Gonnella, Y. He, V. Ho, G. Hoffstaetter, M. Liepe, T. O'Connell, S. Posen, P. Quigley, J. Sears, and V. Veshcherevich, *Proceedings of the 4th International Particle Accelerator Conference, IPAC-2013, Shanghai, China, 2013* (JACoW, Shanghai, China, 2013), p. 2459.

[6] A. Romanenko, A. Grassellino, O. Melnychuk, and D. A. Sergatskov, Dependence of the residual surface resistance of superconducting radio frequency cavities on the cooling dynamics around T_c, J. Appl. Phys. **115**, 184903 (2014).

[7] N. R. A. Valles, R. G. Eichhorn, F. Furuta, G. M. Ge, D. Gonnella, D. L. Hall, Y. He, K. M. V. Ho, G. H. Hoffstaetter, M. Liepe, T. I. O'Connel, S. Posen, P. Quigley, J. Sears, and V. Veshcherevich, *Proceedings of SRF2013, Paris, France* (2013), p. 300.

[8] R. Eichhorn, B. Bullock, B. Clasby, B. Elmore, F. Furuta, M. Ge, D. Gonnella, D. Hall, A. Ganshin, Y. He, V. Ho, G. H. Hoffstaetter, J. Kaufman, M. Liepe, T. O'Connell, S. Posen, P. Qigley, J. Sears, E. Smith, V. Shemelin, and V. Veshcherevich, *Proceedings of SRF2013, Paris, France* (2013), p. 844.

[9] A. C. Crawford, A study of thermocurrent induced magnetic fields in ILC cavities, arXiv:1403.7996.

[10] http://www.thermoelectrics.caltech.edu/thermoelectrics/index.htm.

[11] F. J. Blatt, P. A. Schroeder, C. L. Foiles, and D. Greig, *Thermoelectric Power of Metals* (Plenum Press, New York, 1976).

[12] J.-M. Vogt, O. Kugeler, and J. Knobloch, High-Q operation of superconducting rf cavities: Potential impact of thermocurrents on the rf surface resistance, Phys. Rev. ST Accel. Beams **18**, 042001 (2015).

[13] N. Morton, B. W. James, G. H. Wostenholm, and R. J. Nichols, The electrical resistivity of niobium and niobium-zirconium alloys, Metal Physics **5**, 85 (1975).

[14] W. R. G. Kemp, P. G. Klemens, and G. K. White, Thermal and electrical conductivities of iron, nickel, titanium, and zirconium at low temperatures, Aust. J. Phys. **9**, 180 (1956).

[15] R. Eichhorn, C. Daly, F. Furuta, and A. Ganshin, *Proceedings of IPAC2014, Dresden, Germany* (2014), p. 2621.

[16] G. H. Hoffstaetter, S. Gruner, and M. Tigner, Cornell ERL Updated Project Definition Design Report (2013), http://erl.chess.cornell.edu/PDDR.

[17] R. Eichhorn, B. Bullock, J. V. Conway, B. Elmore, F. Furuta, Y. He, G. H. Hoffstaetter, J. J. Kaufman, M. Liepe, T. I. O'Connel, P. Quigley, D. M. Sabol, J. Sears, E. N. Smith, and V. Veshcherevich, *Proceedings of IPAC2014, Dresden, Germany* (2014), p. 2624.

[18] F. Furuta, B. Bullock, R. G. Eichhorn, B. Elmore, A. Ganshin, M. Ge, G. H. Hoffstaetter, J. Kaufman, M. Liepe, and J. Sears, *Proceedings of SRF2013, Paris, France* (2013), p. 521.

[19] J. M. Vogt, J. Knobloch, and O. Kugeler, *Proceedings of SRF2013, Paris, France* (2013), p. 376.

[20] M. Liepe, R. G. Eichhorn, F. Furuta, G. M. Ge, D. Gonnella, G. H. Hoffstaetter, A. C. Crawford, A. Grassellino, A. Hocker, O. S. Melnychuk, A. Romanenko, A. M. Rowe, D. A. Sergatskov, R. L. Geng, A. D. Palczewski, and C. E. Reece, *Proceedings of IPAC2014, Dresden, Germany* (2014), p. 2627.

[21] J. Halbritter, *Internal Report Forschungszentrum Karlsruhe Report No. KFK-Ext.03/70-06, 1970.*

[22] D. Gonnella and M. Liepe, *Proceedings of IPAC2014, Dresden, Germany* (2014), p. 2631.

[23] D. Gonnella, R. Eichhorn, F. Furuta, M. Ge, D. Hall, V. Ho, G. Hoffstaetter, M. Liepe, T. O'Connell, S. Posen, P. Quigley, J. Sears, V. Veshcherevich, A. Grassellino, A. Romanenko, and D. Sergatskov, Nitrogen-doped 9-cell cavity performance in a test cryomodule for LCLS-II, J. Appl. Phys. **117**, 023908 (2015).

[24] A. Romanenko and A. Grassellino, Dependence of the microwave surface resistance of superconducting niobium on the magnitude of the rf field, Appl. Phys. Lett. **102**, 252603 (2013).

[25] A. Romanenko, *Proceedings of the LINAC2014 conference, Geneva, Switzerland, 2014 (to be published).*

[26] D. Gonnella and M. Liepe, *Proceedings of the LINAC2014 Conference, Geneva, Switzerland, 2014 (to be published).*

[27] N. R. A. Valles, R. Eichhorn, F. Furuta, G. M. Ge, D. Gonnella, D. L. Hall, Y. He, K. M. V. Ho, G. H. Hoffstaetter, M. Liepe, T. I. O'Connel, S. Posen, P. Quigley, J. Sears, and V. Veshcherevich, *Proceedings of SRF2013 Conference, Paris, France* (2013) p. 300.

[28] D. Longuevergne, C. Beard, P. Kolb, R. E. Laxdal, A. Grassellino, and V. Zvyagintsev, *Proceedings of the 25th International Linear Accelerator Conference, LINAC-2010, Tsukuba, Japan* (KEK, Tsukuba, Japan, 2010), p. 860.